Vibration Control of In-Wheel SRM for Electric Vehicle Applications

Wei SUN[1]; Yinong LI[2]; Guangzhong XU[3]; Nong ZHANG[4]

[1] The State Key Laboratory of Mechanical Transmission, Chongqing University, China

[2] The State Key Laboratory of Mechanical Transmission, Chongqing University, China

[3] School of Elec, Mech and Mechatronic Systems, University of Technology Sydney, Australia

[4] School of Elec, Mech and Mechatronic Systems, University of Technology Sydney, Australia

ABSTRACT

The Switched Reluctance Motor (SRM) processes great application potential in In-Wheel Motor (IWM) electric vehicles (EV). However the problem of vibration and noise is always a disadvantage of this kind of motor. By utilizing the analytical Fourier fitting method, a convenience method for modeling In-Wheel Switched Reluctance Motor (IW SRM) is proposed for EV applications. And the negative vibration and noise effect of IW SRM on vehicle is investigated according to the unbalanced residual lateral force. Then corresponding control methods are proposed, modified and compared. The proposed combined vibration feedback control of current chopping with PWM can effectively reduce the SRM residual force and ensure the required vehicle speed, though some small low frequency force response is induced.

Keywords: switched reluctance motor, in-wheel motor, electric vehicle, vibration and shock, vehicle dynamics I-INCE Classification of Subjects Number(s): 13.2.1

1. INTRODUCTION

It now appears that the electric motorization for ground vehicle is an overwhelming tendency in modern automobile industry, and many exhaustive works have been accomplished to improve the propulsion systems for Electric Vehicle (EV).

According to vehicle architecture, these propulsion systems can be generally classified into two categories, the central motor driving layout like conventional internal combustion engine vehicle, as well as the In-Wheel Motor (IWM) driving layout. The IWM is attracting more and more research interests due to its inherent merits, e.g. vehicle packaging innovation, overall weight saving for vehicles, quick and precise torque control as well as independent wheel speed control, and convenience to implement X-by-Wire chassis control system (ABS, TCS or ESP), etc. To maximize these advantages and performance of IWM, a variety of excellent researches have been conducted.

Many types of motors are ready for EV applications, e.g. induction motor, synchronous motor, DC motor as well as Switched Reluctance Motor (SRM). Among these choices, the SRM (1–3) is dedicatedly designed for EV applications with excellent advantages: simple structure and high reliability, favorable torque-speed characteristics, high torque density, high operating efficiency, low starting current. However, these advantages are overshadowed by its high torque ripple, vibration and noise problems, which also seriously hindered the development of SRM for IWM applications.

A variety of different methods have been used to improve the SRM characteristics, such as structure optimization or control algorithm design (4,5). However, the current researches generally aim to improve the SRM driving performance by eliminating the torque ripple induced by the SRM doubly salient structure, and less attention was paid to the effect of In-wheel SRM (IW SRM) on vehicle comfort characteristics.

[1] wsun@cqu.edu.cn
[2] ynli@cqu.edu.cn
[3] guangzhong.xu@gmail.com
[4] Nong.Zhang@uts.edu.au

In light of the above issues, this paper presents an investigation and solution for the vertical and comfort effect of IW SRM on EVs. First an analytical model of SRM is proposed, followed by a preliminary analysis on the torque and unbalanced residual radial force. Then the driving and vibration excitation characteristics of SRM are adopted in a quarter vehicle model and the riding comfort and driving problem are discussed. To address these issues and ensure the drive capability of SRM for EVs, a dual objective control method is proposed and modified. Finally, some key conclusions are presented.

2. SRM characteristics and model

2.1 In-Wheel Switched Reluctance Motor

The IW SRM adopted here is the example introduced by (1,2,6). Figure 1 shows the structure of this IW-SRM. This is an 8/6 - four phases SRM with exterior rotor to meet the IWM requirement. The electrical machine is installed inside wheel hub to realize the direct driving purpose.

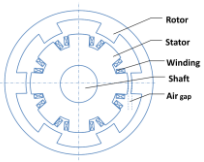

Figure 1 - Structure of exterior rotor 8/6 - four phases SRM for IWM application

2.2 Electromechanical equations

The SRM is a type of reluctance motor in compliance with the minimum reluctance principle: The rotor prefers to come to the minimum reluctance position at the instance of excitation. To generate the adequate reluctance torque, significant radial electromagnetic attractive forces exist between the stator and rotor poles due to the doubly salient structure.

The radial force is a dominant source for the SRM transmitting vibration and noise. Theoretically, these radial forces balance out because the geometrical symmetry and only the modal vibration of motor body and structure-borne noise are transmitted. However, due to the machining or fabrication tolerances, mechanical wear, unbalanced loads and vibration, the motor air gaps are usually asymmetric. As a result, different magnetic pull forces lie between the opposite poles, and the actual net radial force is usually not equal to zero. And because the air gap is small, only a tiny eccentricity will result in a large unbalanced residual radial force. For the IWM EV applications, the unbalanced residual radical force will cause vibration transmitting to both wheels and vehicle body, affecting the vehicle comfort performance.

The phase torque and radial force are

$$T_e = \left.\frac{\partial W_m'}{\partial \theta}\right|_{i=const} = \int_0^i \frac{\partial \psi(\theta, i)}{\partial \theta} di \tag{1}$$

$$F_r = \left.\frac{\partial W_m'}{\partial l_g}\right|_{i=const} = \int_0^i \frac{\partial \psi(\theta, i)}{\partial l_g} di \tag{2}$$

Where W_m' is co-energy, θ represents the relative angular position between stator and rotor, and l_g is airgap. According to Equation (1) and (2), the key to calculate the torque and force is to acquire the flux linkage characteristics of the SRM. While the flux linkage is determined by inductance and current, the electromagnetic equations and circuit equations are employed.

2.3 Electromagnetic equations

Assume the unaligned position between rotor and stator is the initial position, i.e. 0 degree. Then the aligned position is π/N_r. The inductance corresponding to rotor angular position and winding current could be written in Fourier series (7,8)

$$L_k(\theta, i_k) = \sum_{n=0}^{\infty} L_n(i_k) \cos(nN_r\theta + \varphi_n) \tag{3}$$

Where, $\varphi_n = n\pi$

The Fourier coefficients L_n related to winding current could be deduced by inductance at the aligned, unaligned and other position (9).

Ignoring the higher order harmonics, sufficient accuracy could be obtained by 3rd order Fourier series, and the aligned, unaligned and midway inductance are used (10)

$$L_0(i) = \frac{1}{2}\left[\frac{1}{2}(L_a + L_u) + L_m\right] \tag{4}$$

$$L_1(i) = \frac{1}{2}(L_a - L_u) \tag{5}$$

$$L_2(i) = \frac{1}{2}\left[\frac{1}{2}(L_a + L_u) - L_m\right] \tag{6}$$

Where the inductance at the unaligned position could be assumed as a constant due to the relative large air gap (11), and the inductance at the aligned and midway position could be expressed by polynomial function of winding current, and cubic polynomial is adequate

$$L_a(i)|_{\theta=\frac{\pi}{N_r}} = \sum_{n=0}^{N} a_n i^n \tag{7}$$

$$L_m(i)|_{\theta=\frac{\pi}{2N_r}} = \sum_{n=0}^{N} b_n i^n \tag{8}$$

Then the inductance of phase k is

$$L_k(\theta, i_k) = \frac{1}{2}[\cos^2(N_r\theta) - \cos(N_r\theta)] \sum_{n=0}^{N} a_n i_k^n + \sin^2(N_r\theta) \sum_{n=0}^{N} b_n i_k^n + \frac{1}{2} L_u [\cos^2(N_r\theta) + \cos(N_r\theta)] \tag{9}$$

Since the inductance is the partial differential equation of flux linkage to winding current (6), the flux linkage of phase k is

$$\psi(\theta, i_k) = \int_0^{i_k} L_k(\theta, i_k)\, di_k = \frac{1}{2}[\cos^2(N_r\theta) - \cos(N_r\theta)] \sum_{n=0}^{N} c_n i^n + \sin^2(N_r\theta) \sum_{n=0}^{N} d_n i^n + \frac{1}{2} L_u i_k [\cos^2(N_r\theta) + \cos(N_r\theta)] \tag{10}$$

Where $c_n = \frac{a_{n-1}}{n}$ and $d_n = \frac{b_{n-1}}{n}$ are the Integral coefficients for the a_n and b_n. Due to the continuity, $c_0 = d_0 = 0$.

It can be concluded that the flux linkage is also a Fourier series model of rotor angular position and winding current. The original data for fitting is referred to (2,3), which is acquired by FEA method. The fitted flux linkage characteristics and calculated inductance are shown as Figure 2. It can be seen that the Fourier fitted results agree well with the original flux linkage data, which valid this method of analytical Fourier fitting expression for modeling a SRM.

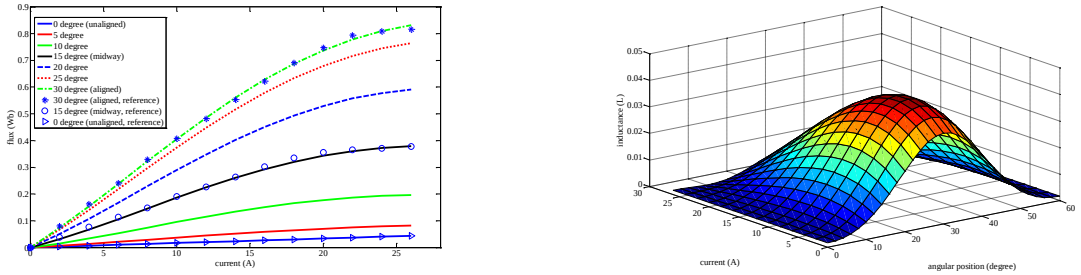

(a) Phase flux linkage profile (b) Phase inductance distributions

Figure 2 - Statics electromagnetic characteristics of the SRM

2.4 Mechanical equations

According to Equation (10), there is

$$\frac{\partial\psi(\theta,i_k)}{\partial\theta}=\sin(N_r\theta)\sum_{n=0}^{N}e_n i_k^n+\sin(2N_r\theta)\sum_{n=0}^{N}f_n i_k^n \tag{11}$$

Where

$e_n=\frac{1}{2}N_r c_n$, $e_0=0$, $e_1=\frac{1}{2}N_r(c_1-L_u)$

$f_n=N_r d_n-e_n$, $f_0=0$, $f_1=\frac{1}{2}N_r(2d_1-c_1-L_u)$

Substituting Equation (11) into Equation (1), the torque of phase k is

$$T_k=\int_0^{i_k}\frac{\partial\psi(\theta,i_k)}{\partial\theta}di_k=\sin(N_r\theta)\sum_{n=1}^{N}\frac{1}{n}e_{n-1}i_k^n+\sin(2N_r\theta)\sum_{n=1}^{N}\frac{1}{n}f_{n-1}i_k^n \tag{12}$$

The torque at different rotor position varying with winding current is shown in Figure 3(a). Generally, the output torque of SRM reaches the maximum in the aligned position, but in the actual condition, the current is pulsing in a conducting cycle. So the control of SRM is to optimize the conducting state of SRM phase, make the current in appropriate wave form so that the SRM can output a desired, continuous, smooth torque with minimal vibration.

Similarly the radial electromagnetic attractive force between rotor and stator poles could be obtained. By neglecting the fringing flux and mutual inductance, the radial force can be simplified as (12)

$$F_{rk}=-\frac{1}{2}i_k^2\frac{L_k(\theta,i_k)}{l_g} \tag{13}$$

Where, the negative sign means the rotor is approaching toward the stator.

Define the relative eccentricity as

$$\varepsilon=h_e/l_g$$

Where, l_g is the radial airgap length in the case of no eccentricity and h_e is the eccentricity in the radial direction. In the actual situation, the maximum expected relative eccentricity can achieve 30%-60% (13,14).

Then the unbalanced residual radial force of phase k is

$$F_{rk}=F_{rm}-F_{rn}=\frac{1}{2}i^2\frac{L_k(\theta,i_k)}{l_g(n)}-\frac{1}{2}i^2\frac{L_k(\theta+\pi,i_k)}{l_g(m)} \tag{14}$$

Where m, n is the pole number of stator in opposite direction, according to the 8/6 SRM structure in this paper, $|m-n|=4$.

The radial forces are shown in Figure 3(b). It can be seen the radial attraction force between stator and rotor poles can be very large even with small current. Though radial attraction force falls down when current exceed a specific value, the unbalanced residual radial force is still considerable. And the eccentricity has dominant influence on the unbalanced residual radial force, which increase sharply with the eccentricity.

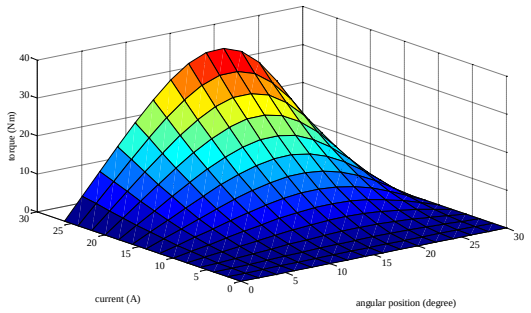

(a) Output torque related to rotor position and winding current

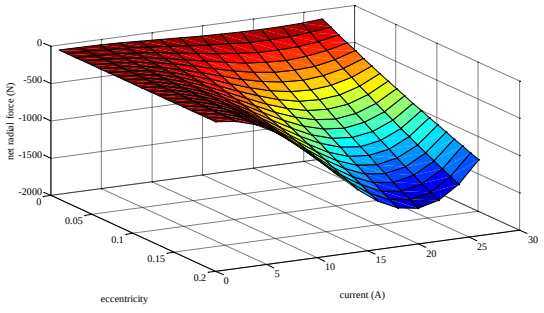

(b) Peak value of unbalanced residual radial force related to winding current and eccentricity

Figure 3 - Statics mechanical characteristics of the SRM

2.5 Circuit equations

The instantaneous voltage across the terminals of a SRM phase winding is related to the flux linkage in this winding by Faraday's law

$$U_k = R_k i_k + \frac{d\psi_k}{dt} \tag{15}$$

According equation (10), the flux linkage is a function of rotor position θ and the phase current i_k. So Equation (15) can be rewritten as (15)

$$U_k = R_k i_k + \frac{d\psi_k}{dt} = R_k i_k + \frac{\partial \psi_k}{\partial i_k}\frac{di_k}{dt} + \frac{\partial \psi_k}{\partial \theta}\frac{d\theta}{dt} = R_k i_k + L_k(\theta, i_k)\frac{di_k}{dt} + \omega\frac{\partial \psi(\theta, i_k)}{\partial \theta} \tag{16}$$

Then

$$i_k = \int \frac{U_k - R_k i_k - \omega\frac{\partial \psi(\theta, i_k)}{\partial \theta}}{L_k(\theta, i_k)} dt \tag{17}$$

Substitute the Equation (9) and (11) into the Equation (17), the current response can be obtained.

3. IW SRM effect on vehicle dynamics

To analyze the impact of SRM IWM on vehicle, hereby a quarter vehicle model emphases on driving and vertical vibration is adopted. And the eccentricity is applied on only one phase of the SRM for simplicity. As a result, an additional force exerts on the wheel vertically and impulsively. As shown in Figure 4.

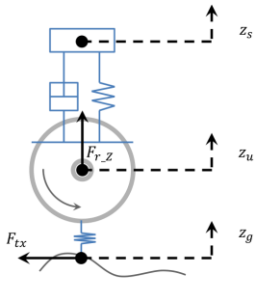

Figure 4 - Quarter vehicle model with SRM driving

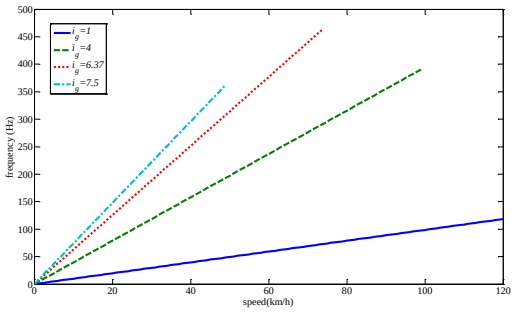

Figure 5 - Relationship between vehicle speed and SRM excitation frequency

3.1 IW SRM driving quarter vehicle modeling

3.1.1 Driving equations

The motion of wheel is defined by the following equation

$$\frac{I_t\dot{\omega}}{i_g} = \eta i_g T_e - F_{tx}R_e - M_t \tag{22}$$

Where, $\dot{\omega}$ is the wheel angular speed, η is the transmission efficiency, i_g is the transmission ratio, and M_{ty} is the rolling resistance moment. The reaction force F_{tx} from ground to tire can be acquired through Magic Formula.

3.1.2 Vibration equations

The vibration equations of sprung and unsprung mass are

$$m_s\ddot{z}_s = k_s(z_u - z_s) + c_s(\dot{z}_u - \dot{z}_s) \tag{23}$$

$$m_u\ddot{z}_u = k_t(z_g - z_u) - k_s(z_u - z_s) + c_t(\dot{z}_g - \dot{z}_u) - c_s(\dot{z}_u - \dot{z}_s) + F_{r\_Z}$$

Where, m_u and m_s are the unsprung and sprung mass. k_s and $k_t$are suspension and tire stiffness, c_s and $c_t$are suspension and tire damping. F_{r_Z} is the unbalanced residual lateral force of motor. z_g, z_u and z_s represent the displacement of ground, unsprung mass and sprung mass. The road roughness can be expressed by the filtered white noise model.

3.2 Analysis of IW SRM effect on vehicle

The excitation frequency of the IW SRM is

$$f_e = i_g \frac{n_v}{60} N_r = i_g \frac{\omega}{2\pi} N_r \cong i_g \frac{v}{2\pi R_e} N_r = i_g \frac{v_{(km/h)}}{2\pi R_e} \frac{N_r}{3.6} \tag{26}$$

Where, n_v is the motor speed in RPM, i_g is the transmission ratio. In this case, the rated rotational speed of the SRM is 30-2000 RPM. The excitation frequency according to different speed and transmission ratio is shown as Figure 5. It can be seen that in the commonly used speed range (30-80km/h), depending on different gear ratio, the excitation frequency may lie in a low range of 30-80Hz, which easily arises harmful low frequency noise, or in a high range of 400-600Hz, which is annoying and very closed to the tire noise resonance frequency (16). , In this paper the i_g is optimized to 6.37 to amplify the SRM torque for vehicle acceleration requirement, and the frequency of the excitation radial force lies in the tire noise frequency range.

4. Controller design and results analysis

4.1 Controller design

In this paper, the PWM is the fundamental control method for its favorable controllability in large speed range, and the turn-on angle of 5.5 degree and turn-off angle of 25 degree are fixed. There will be no negative effect on vehicle if the SRM is ideal. But with the assumption of eccentricity in one phase of SRM, the aforementioned vibration problem will occur. Because the magnetic attraction force is due to the winding current, the CCC is also adopted to eliminate the undesirable vibration response and a combined control method of CCC and PWM is proposed (control method 1). However, though limiting the current peak value can reduce the vibration response, the effective output torque is also suppressed. To guarantee the necessary torque for vehicle speed requirement, the proposed combined control method is modified, only the faulted phase current is chopped (control method 2). The work condition of constant speed of 15m/s on a B class road is investigated. The relative eccentricity is set to 10%, a moderate case. Main results are shown in Figure 6, as well as Table 1.

4.2 Control results analysis

The control results are shown in Figure 6. According to control method 1, due to the limited windings current, the SRM output torque is also reduced and the speed is unsatisfactory. The duty cycle of PWM drive increased, but still cannot compensate the torque loss and speed dropdown. With the modified control method (control method 2), only the faulted phase current is limited, it can be seen the speed requirement can be fulfilled, with less change in the average torque and duty cycle.

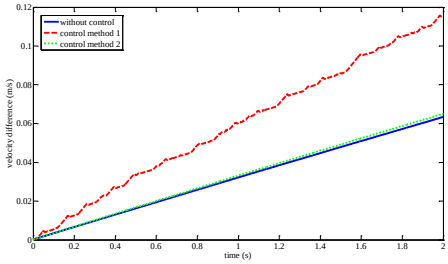

(a) Speed error in constant speed condition

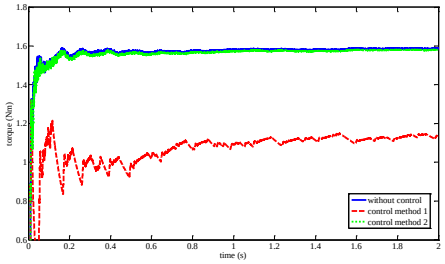

(b) Average output torque in constant speed

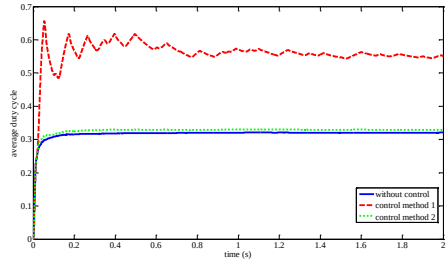

(c) Average duty cycle in constant speed condition

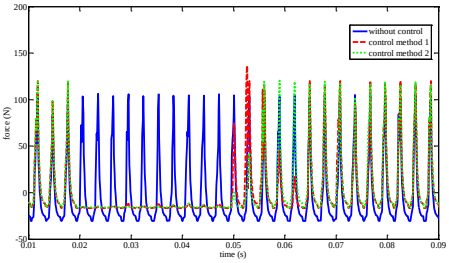

(d) Residual force of SRM in constant speed condition

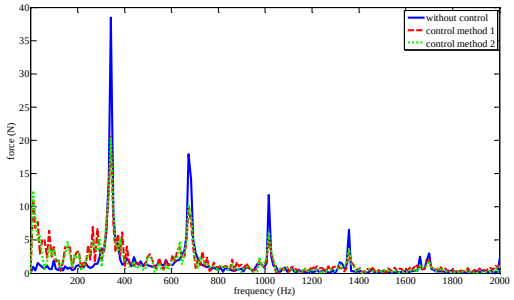

(e) FFT of residual SRM force in constant speed condition
Figure 6 - Control results comparison in constant speed condition

Table 1 - Control results comparison of vibration and force response in constant speed condition

	RMS acceleration of Sprung mass m/s^2 (%)	RMS dynamic deflection of suspension mm (%)	RMS dynamic deflection of tire (%)	RMS dynamic residual force N (%)
Without control	0.26	1.795	0.814	48.46
Control 1	0.256 (-1.5%)	1.789 (-0.3%)	0.813 (-0.1%)	35.27 (-27.2%)
Control 2	0.257 (-1.1%)	1.795 (0%)	0.82 (+0.7%)	35.21 (-27.3%)

For the vibration response, the effect of SRM force on vehicle vibration is implicit because of the relative high excitation frequency. So the residual force will be the key control objective. And the results are listed in Table 1 and Figure 7.

According to Table 1, the control methods have limited effect on the RMS value of different vibration response because the major excitation in this condition is from road. But a significant reduction for the RMS value of SRM residual force, which decreased from 48.46 N to around 35 N, a reduction of about -27%, can be observed. And the Figure 7(d) also illustrates the comparison between different control methods. It can be seen, the control results of the two methods show minute difference, which may because of the relative small torque and current requirements in this constant speed condition and less current are chopped. But both of the two feedback control methods can cut off the force excitation periodically, also increase the mean force value and adjust the fluctuation axis, which make the fluctuation more concentrate. All of these are helpful to reduce the force RMS value and noise excitation.

Besides, as shown in Figure 7(e), high frequency force components are attenuated effectively, which may contribute to the noise reduction. However, with the periodical cutoff of winding current and unbalanced residual lateral force, some low frequency excitations can be aroused. These low frequency excitations may deteriorate the tire dynamic load, and reduce vehicle driving stability. Fortunately, the low frequency components are relative small, equivalent to 1-1.5 kg attached vibration mass on the wheel, which is relatively a small increment compare to the IWM applications (usually about 30 kg).

5. Conclusions

By utilizing the analytical Fourier fitting method, an In-Wheel Switched Reluctance Motor (IW SRM) is modelled for electric vehicle applications in this paper. And the characteristics of the output torque and unbalanced residual lateral force related to rotor angular position and winding current are analyzed. The negative effect and control method of IW SRM for electric vehicle are investigated. And some crucial conclusions are drawn.

1. The unbalanced residual lateral force from SRM will have a negative effect on the vehicle vertical dynamics and noise characteristics. The eccentricity has great influence on the unbalanced residual lateral force of SRM. Within the engineering allowance, magnitude of kilo newton residual force can be generated. But in the actual situation, this force is a relative high frequency periodic pulse excitation. According to different gear ratios, the vibration frequency range that the force can cover is

also different. In middle or high speed conditions, the excitation frequency is within the tire noise frequency range, which may increase the vehicle noise resonance.

2. According to the proposed control method, the combined vibration feedback control of current chopping with PWM can effectively reduce the SRM residual force for vehicle. But a simple current chopping will limit the output torque of SRM, and result in the speed loss of vehicle. A modified current chopping focus on faulted phase can avoid this issue. Both of the two current chopping methods can effectively cut off the high frequency component of SRM residual force, but induce low frequency force response, which is against to vehicle wheel bounce and vehicle stability. Fortunately, the magnitude of the induced low frequency force is small.

ACKNOWLEDGEMENTS

This work was supported by National Natural Science Foundation of China (Grant No. 51275541), Natural Science Foundation of Chongqing (Grant No. CSTC2013jjB0022), Foundation of State Key Laboratory of Mechanical Transmission (Grant No. SKLMT-ZZKT-2012 ZD 06) and the China Scholarship Council.

REFERENCES

1. Jiongkang Lin, Cheng EKW, Zhu Zhang, Xiangdang Xue. Experimental investigation of in-wheel switched reluctance motor driving system for future electric vehicles. 2009. p. 1–6.
2. Xue XD, Cheng KWE, Lin JK, Zhang Z, Luk KF, Ng TW, et al. Optimal Control Method of Motoring Operation for SRM Drives in Electric Vehicles. IEEE Trans. Veh. Technol. 2010 Mar;59(3):1191–204.
3. Wong KF, Cheng KWE, Ho SL. Simulation of Switched Reluctance Motor Based on a Combination of Circuit-oriented and Signal-oriented Approaches Using Matlab/SimPowerSystems. Electr. Power Components Syst. Taylor & Francis; 2007 Feb;35(2):205–19.
4. Chen L, Hofmann W. Speed Regulation Technique of One Bearingless 8/6 Switched Reluctance Motor With Simpler Single Winding Structure. IEEE Trans. Ind. Electron. 2012 Jun;59(6):2592–600.
5. Faiz J, Soltani-Khosroshahi G. Torque Ripple Minimization in Switched Reluctance Motor by Optimal Commutation Strategy Using a Novel Reference Torque. Electr. Power Components Syst. Taylor & Francis; 2002 Jul;30(7):769–82.
6. Xue XD, Cheng KWE, Ng TW, Cheung NC. Multi-Objective Optimization Design of In-Wheel Switched Reluctance Motors in Electric Vehicles. IEEE Trans. Ind. Electron. 2010 Sep;57(9):2980–7.
7. Fahimi B, Suresh G, Mahdavi J, Ehsami M. A new approach to model switched reluctance motor drive application to dynamic performance prediction, control and design. PESC 98 Rec. 29th Annu. IEEE Power Electron. Spec. Conf. (Cat. No.98CH36196). IEEE; 1998. p. 2097–102.
8. Husain I, Ehsani M. Torque ripple minimization in switched reluctance motor drives by PWM current control. IEEE Trans. Power Electron. 1996;11(1):83–8.
9. Ye ZZ, Martin TW, Balda JC. Modeling and nonlinear control of a switched reluctance motor to minimize torque ripple. SMC 2000 Conf. Proceedings. 2000 IEEE Int. Conf. Syst. Man Cybern. 'Cybernetics Evol. to Syst. Humans, Organ. their Complex Interact. (Cat. No.00CH37166). IEEE; 2000. p. 3471–8.
10. Mahdavi J, Suresh G, Fahimi B, Ehsani M. Dynamic modeling of nonlinear SRM drive with Pspice. IAS '97. Conf. Rec. 1997 IEEE Ind. Appl. Conf. Thirty-Second IAS Annu. Meet. IEEE; 1997. p. 661–7.
11. Krishnamurthy M, Edrington CS, Emadi A, Asadi P, Ehsani M, Fahimi B. Making the case for applications of switched reluctance motor technology in automotive products. IEEE Trans. Power Electron. 2006 May;21(3):659–75.
12. Cameron DE, Lang JH, Umans SD. The origin of acoustic noise in variable-reluctance motors. Conf. Rec. IEEE Ind. Appl. Soc. Annu. Meet. IEEE; 1989. p. 108–15.
13. Ayari S, Besbes M, Lecrivain M, Gabsi M. Effects of the airgap eccentricity on the SRM vibrations. IEEE Int. Electr. Mach. Drives Conf. IEMDC'99. Proc. (Cat. No.99EX272). IEEE; 1999. p. 138–40.
14. Garrigan NR, Soong WL, Stephens CM, Storace A, Lipo TA. Radial force characteristics of a switched reluctance machine. Conf. Rec. 1999 IEEE Ind. Appl. Conf. Thirty-Forth IAS Annu. Meet. (Cat. No.99CH36370). IEEE; 1999. p. 2250–8.
15. Sahoo SK, Dasgupta S, Panda SK. A Lyapunov Function-Based Robust Direct Torque Controller for a Switched Reluctance Motor Drive System. IEEE Trans. Power Electron. 2012 Feb;27(2):555–64.
16. Iwao K, Yamazaki I. A study on the mechanism of tire/road noise. JSAE Rev. 1996;17(2):139–44.

Appendix - Key nomenclature and value

Symbol	Value	Unit	Note
$k = a, b, c, \cdots$			Subscript indicates phase $a, b, c, \cdots$
ψ_k			Flux linkage of phase k
θ			Rotor angular position
T_e			Motor output torque
T_k			Motor torque of phase k
F_r			Motor radial force
F_{rk}			Motor radial force of phase k
F_{r_Z}			Unbalanced residual force applied on vehicle vertically
F_{tx}			Reaction driving force from ground to tire
L_k			Inductance of phase k
L_a			Inductance at aligned position
L_m			Inductance at midway position
L_u	1.67	mH	Inductance at unaligned position
l_g	0.5	Mm	Radial airgap (between rotor and stator poles)
N_r	6		Number of rotor poles
N_s	8		Number of stator poles
ε			Relative eccentricity
h_e			Eccentricity in the radial direction
U_k			Voltage applied on phase k
i_k			Winding current of phase k
R_k	0.678	mΩ	Winding resistance of phase k
v			Vehicle speed
f_r	0.013		rolling resistance coefficient
i_g	6.37		Transmission ratio
R_e	269	mm	Effective radius of the wheel
I_t	1.2	kg.m^2	Wheel moment of inertia
m_s	337.5	kg	Sprung mass
m_u	65	kg	Unsprung mass
k_t	250000	N/m	Tire stiffness
k_s	22500	N/m	Suspension stiffness
c_t	375	N.s/m	Tire damping
c_s	1450	N.s/m	Suspension damping